Materials Advances

ROYAL SOCIETY OF CHEMISTRY

PAPER

View Article Online
View Journal | View Issue

Check for updates

Cite this: *Mater. Adv.*, 2022, 3, 3906

Structure–gelation property relationships of phenolic glycosides of pentose sugars: pH dependent controlled release of curcumin†

Navendu P. Pathak,[a] Arunava Sengupta[b] and Somnath Yadav *[a]

Received 30th September 2021,
Accepted 15th March 2022

DOI: 10.1039/d1ma00907a

rsc.li/materials-advances

Herein, we explored a library of structurally simple phenolic glycopyranosides of pentose sugars as organogelators, with the objective of finding a correlation between the sugar configuration and gelation ability. Of the twenty eight compounds investigated, only four–two each from the β-arabino- and α-xylo-series – were found to be capable of acting as organogelators. Thorough characterization of supramolecular gels using techniques such as FESEM, AFM, rheology, FTIR spectroscopy and WXRD led to the identification of one arabinoside derivative as being able to form the most mechanically robust organogel at loadings of about 0.2–0.3% (w/v). The mechanism of self-assembly involved mainly H-bonding interactions as evidenced from FTIR spectroscopy, WXRD and theoretical studies, although some evidence of π–π stacking interactions was also observed. This gelator was then used to prepare a curcumin entrapped organogel in mustard oil that was explored for the pH dependent controlled release of a drug model – curcumin.

Open Access Article. Published on 18 March 2022. Downloaded on 2/8/2026 1:46:29 AM.
This article is licensed under a Creative Commons Attribution-NonCommercial 3.0 Unported Licence.

Introduction

The design and synthesis of low molecular weight gelators capable of forming soft materials through self-assembly have gained attention over the past two decades.[1,2] A lot of results in this direction have been obtained from the studies on the structure–property relationships at the molecular level for understanding the parameters that lead to self-assembly.[3,4] Among the various categories of molecules that have been used for the synthesis of low molecular weight gelators, carbohydrates are unique as biocompatible and easily available precursors for the design and synthesis of supramolecular gelators.[5,6] This stems from the fact that multiple hydroxyl groups provide the opportunity for self-assembly through hydrogen bonding interactions. Together with this, a balance of hydrophobicity can be easily provided by a plethora of protecting group manipulations using the well-established chemistry of carbohydrate synthesis. This strategy has been successfully implemented in the reports of a variety of carbohydrate based hydrogelators as well as organogelators.[3,7] In designing carbohydrate based gelators, several aspects have to be taken into account such as the sugar configuration and the anomeric configuration.[8,9] Such configuration dependent gelation abilities have been investigated and reported by Shinkai and co-workers for hexose sugars.[3,7–10] They synthesized and investigated the gelation property–structure relationship of both the anomers of 4,6-benzylidene derivatives of the methyl glycosides of some hexose sugars. The authors found that the gelation abilities varied with the monosaccharide sugar configuration among the hexoses as well as the anomeric configuration of a particular sugar. These conclusions contributed to the design of gelators using particular hexose sugars as can be seen in the reports of several 4,6-arylidine derivatives of glucose for diverse applications.[11–19] However, such fundamental investigations into the structure–property relationships of other classes of sugars are severely limited. We had previously reported a simple phenolic glycoside of arabinose as an organogelator[20] as part of our ongoing work on the design of arabinose based gelators.[21–23] To gain a better understanding of the structure–gelation property relationship of these classes of monosaccharides, we have investigated and herein report the same for the phenolic glycosides of pentose sugars (Fig. 1). Furthermore, we have used the most effective organogelator for the controlled release of curcumin from biocompatible and edible vegetable oil at different pH values.

Results and discussion

Synthesis of the library of phenolic glycosides of pentose sugars

A library of phenolic glycosides of the aldopentose sugars (D-arabinose, D-xylose, D-lyxose and D-ribose) were synthesized as depicted in Scheme 1 from tetra-*O*-acetylpyranose precursors.

[a] *Department of Chemistry, Indian Institute of Technology (ISM), Dhanbad, 826004, Jharkhand, India. E-mail: somnath@iitism.ac.in*
[b] *Department of Chemistry, Techno India University, Kolkata, 700091, West Bengal, India*

† Electronic supplementary information (ESI) available: Additional figures and 1H and 13C NMR spectra of all compounds. See DOI: 10.1039/d1ma00907a

© 2022 The Author(s). Published by the Royal Society of Chemistry

Open Access Article. Published on 18 March 2022. Downloaded on 2/8/2026 1:46:29 AM.
This article is licensed under a Creative Commons Attribution-NonCommercial 3.0 Unported Licence.

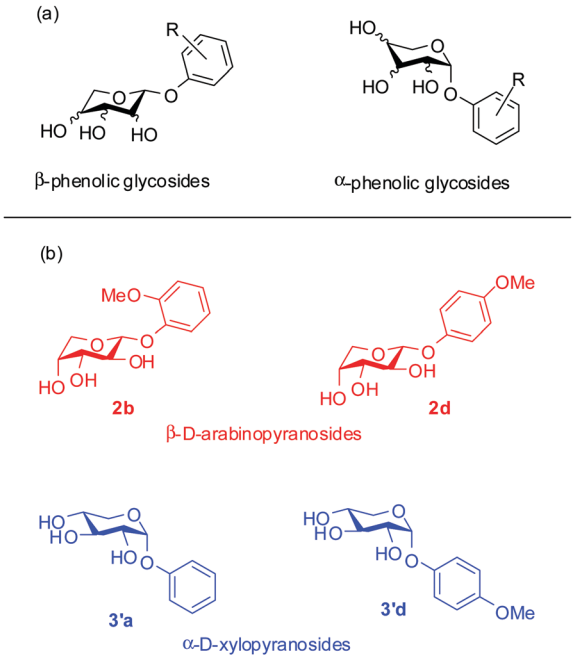

Fig. 1 (a) The library of phenolic glycosides of pentose sugars reported in this study. (b) Structures of the organogelators.

For the β-isomers **2a–d**, **3a–d** and **4a–d**, the tetra-*O*-acetylpyranose precursors were treated with phosphorus tribromide to yield the corresponding anomeric bromides. This was then followed by treatment of the anomeric bromide with the corresponding sodium phenolate obtained by the reaction of phenol with NaH. Finally, global deprotection of the acetyl groups was carried out using a catalytic amount of sodium methoxide (NaOMe) in methanol to afford the desired β-isomers of the phenyl glycosides **2–4** in 23–50% yields over three steps. However, this method did not produce the desired product with ribose. The α-isomers of the phenyl glycosides were synthesized by treatment of the tetra-*O*-acetylpyranose precursors with the corresponding phenol in the presence of a catalytic amount of triflic acid, followed by global de-acetylation as above to afford the desired α-isomers of the phenyl glycosides **2′–4′** in 41–88% yields over two steps. However, this method did not produce the desired α-product with ribose, probably as it isomerized to the β-isomer **5** in solution. All the products were characterized in detail using spectroscopic techniques such as FTIR spectroscopy, ^{1}H- and ^{13}C-NMR spectroscopy, HRMS and specific rotation (see the ESI† for detailed characterization data).

Gelation properties

Gelation tests for all the synthesized compounds were carried out in a variety of solvents using the standard vial inversion method. For this purpose, a weighed amount of phenyl glycoside was taken in a 5 mL vial and dissolved in a particular solvent by mild heating. Then, the vial was allowed to stand at room temperature after which it was inverted to check for gelation. From the experiments, it was found that in addition to the previously reported compound, 1-(2-methoxyphenoxy)-β-D-arabinopyranoside (**2b**),[20] the β-arabinopyranoside, 1-(4-methoxyphenoxy)-β-D-arabinopyranoside (**2d**) and α-xylopyranosides, 1-(phenoxy)-α-D-xylopyranoside (**3′a**) and 1-(4-methoxyphenoxy)-α-D-xylopyranoside (**3′d**) were effective gelators for common hydrocarbon based organic solvents (Table 1). Additionally, compound **2b** was able to gel amyl alcohol. An exhaustive list of the solvents tested for gelation with all the synthesized compounds is presented in the ESI† (Tables S1 and S2). In general, for compound **2b**, the minimum gelator concentration (MGC) typically was 0.2% (w/v), while, for **2d**, the MGCs typically ranged from 0.3% to 0.5% (w/v) for the solvents it was able to gel. For compound **3′a**, the MGCs ranged from 0.5% to 0.8% (w/v) and, for **3′d**, the MGCs ranged from 0.3% to 0.5% (w/v). Additionally, the gelation of the compounds was also tested for different edible and cosmetic vegetable oils such as mustard oil, coconut oil and olive oil. It was found that **2b** was able to form gels in mustard oil (MGC = 1% w/v) and coconut oil (MGC = 0.3% w/v), while **2d**, **3′a** and **3′d** formed gels only with coconut oil.

From these results, it can be concluded within certain limitations that among the phenolic glycosides of the pentose sugars in the pyranose form only β-arabinosides and α-xylosides were able to form gels. Again the gelation abilities were also dependent on the substituents on the phenols. While the xyloside of simple phenol was able to form weak gels, stronger gels in the arabino- and xylo-series were formed by the *ortho*- and *para*-methoxy derivatives.

Microstructural characterization of the gels

To gain insight into the microstructure of organogels, field emission scanning electron micrographs (FESEM) of the corresponding *p*-xylene xerogels of the gelators were also obtained. From the micrographs, it was observed that **2b** self-assembled through a fibrillar network (Fig. 2a) with well defined thin fibres. The gelator **2d** also self-assembled through fibres, but the fibres were thicker (Fig. 2b). In contrast, organogelators **3′a** and **3′d** self-assembled in sheet like manners (Fig. 2c and d). The gels were also characterized through atomic force microscopy studies which revealed that the morphology of the gel microstructures correalted well with those observed from the FESEM experiments.

Mechanical properties of the gels

To compare the mechanical properties of different gels, rheological experiments were carried out at 1% (w/v) concentration of the gelators in the same solvent – *p*-xylene. For each of the gels of **2b**, **2d**, **3′a** and **3′d** in *p*-xylene, two separate experiments were carried out *viz.* (i) dynamic strain sweep (DSS) experiments and (ii) dynamic frequency sweep (DFS) experiments (Fig. S5–S8, ESI†). The DSS experiments at a constant frequency quantify the limiting strain (depicted by γ) beyond which the gel transitions from a visco-elastic solid like material to a fluid like material, providing the opportunity to compare the mechanical strength of the gels from different gelators in an identical solvent. From a comparison of the values of γ (Table 2) for each of the gels from gelators **2b**, **2d**, **3′a** and **3′d** in *p*-xylene, it can be clearly seen that **2b** (γ = 0.2822%) formed the mechanically most robust gel as

Open Access Article. Published on 18 March 2022. Downloaded on 2/8/2026 1:46:29 AM.
This article is licensed under a Creative Commons Attribution-NonCommercial 3.0 Unported Licence.

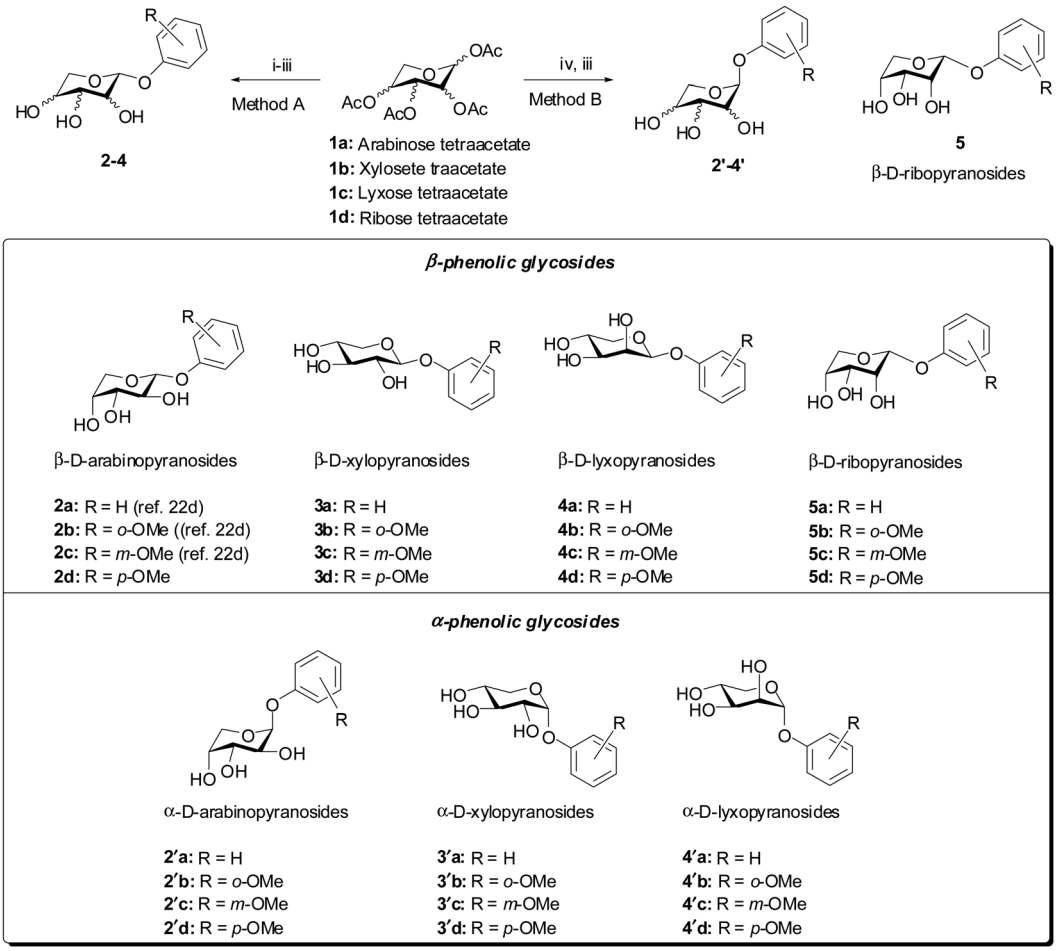

Scheme 1 Synthesis of phenolic glycosides of pentose sugars – arabinose, xylose, lyxose and ribose. Reagents and conditions: (i) PBr_3, AcOH, RT, 4 h, (ii) NaH, ArOH, DMF, 6 h, (iii) NaOMe (cat.), MeOH, RT, 1 h, and (iv) ArOH, DCM, TfOH (cat.), 0–25 °C, 6 h.

Table 1 Gelation properties of phenolic glycoside derivatives **2b**, **2d**, **3′a**, and **3′d**[a]

Solvent	**2b** (MGC[b], T_g[c])	**2d** (MGC[b], T_g[c])	**3′a** (MGC[b], T_g[c])	**3′d** (MGC[b], T_g[c])
Benzene	G, (0.2%, 58–59 °C)	G, (0.3%, 52–53 °C)	G, (0.7%, 54–55 °C)	G, (0.3%, 48–49 °C)
Toluene	G, (0.2%, 61–62 °C)	G, (0.3%, 60–61 °C)	G, (0.5%, 57–58 °C)	G, (0.5%, 58–59 °C)
o-Xylene	G, (0.2%, 67–68 °C)	G, (0.5%, 60–61 °C)	G, (0.8%, 58–59 °C)	G, (0.3%, 56–57 °C)
m-Xylene	G, (0.2%, 68–69 °C)	G, (0.5%, 65–66 °C)	G, (0.8%, 63–64 °C)	G, (0.3%, 60–61 °C)
p-Xylene	G, (0.2%, 70–71 °C)	G, (0.5%, 59–60 °C)	G, (0.8%, 56–57 °C)	G, (0.3%, 59–60 °C)
Chlorobenzene	G, (0.2%, 64–65 °C)	G, (0.5%, 58–59 °C)	G, (0.5%, 55–56 °C)	G, (0.5%, 63–64 °C)
Amyl alcohol	G (1%, 52–53 °C)	S	S	S
n-Butyl alcohol	S	S	S	S
Methanol	S	S	S	S
Ethanol	S	S	S	S
Water	S	S	S	S
DMF	S	S	S	S
DMSO	S	S	S	S
Coconut oil	G (0.3%, 61–62 °C)	G (0.5%, 58–59 °C)	G (0.6%, 54–55 °C)	G (0.5%, 60–61 °C)
Mustard oil	G (1%, 55–56 °C)	PG	PG	PG
Olive oil	PG	S	S	S

[a] G = gel; PG = partial gel; S = solution; PS = partially soluble. [b] MGC = minumum gelation concentration % (w/v). [c] T_g = gelation temperature.

compared to **2d** (γ = 0.0713%), **3′a** (γ = 0.0445%), and **3′d** (γ = 0.0245%). The above conclusions were also reinforced by the DFS experiments, the graphs from which represent the linear visco-elastic region at which the gels are stable. From the DFS experiments, the tan δ values of the gels could also be calculated. The tan δ value reflects the ratio of the loss modulus (G'') to the

© 2022 The Author(s). Published by the Royal Society of Chemistry

Open Access Article. Published on 18 March 2022. Downloaded on 2/8/2026 1:46:29 AM.
This article is licensed under a Creative Commons Attribution-NonCommercial 3.0 Unported Licence.

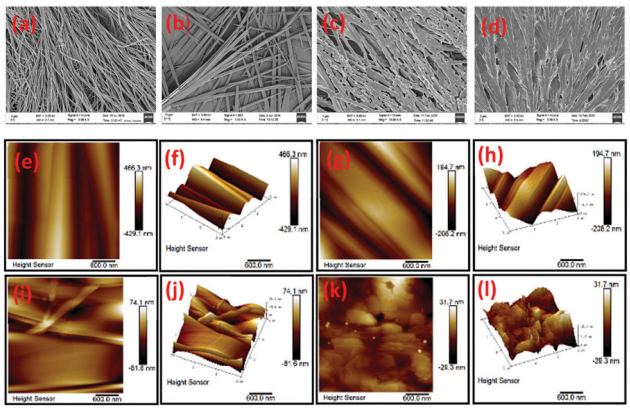

Fig. 2 (a) FESEM image of the *p*-xylene xerogel of **2b**. (b) FESEM image of the *p*-xylene xerogel of **2d**. (c) FESEM image of the *p*-xylene xerogel of **3′a**. (d) FESEM image of the *p*-xylene xerogel of **3′d**. (e) 2D AFM image of the *p*-xylene xerogel of **2b**. (f) 3D AFM image of the *p*-xylene xerogel of **2b**. (g) 2D AFM image of the *p*-xylene xerogel of **2d**. (h) 3D AFM image of the *p*-xylene xerogel of **2d**. (i) 2D AFM image of the *p*-xylene xerogel of **3′a**. (j) 3D AFM image of the *p*-xylene xerogel of **3′a**. (k) 2D AFM image of the *p*-xylene xerogel of **3′d**. (l) 3D AFM image of the *p*-xylene xerogel of **3′d**.

Table 2 Rheological properties of the *p*-xylene gels of **2b**, **2d**, **3′a**, and **3′d**

Organogelator	$G' \times 10^4$ (Pa)[a]	$G'' \times 10^3$ (Pa)[b]	$\gamma \times 10^{-2}$ (%)	Tan δ[c]
2b	41.08	4.51	28.22	0.11
2d	17.13	7.48	7.13	0.43
3′a	24.43	9.61	4.55	0.31
3′d	61.08	17.24	2.45	0.47

[a] G' = storage modulus. [b] G'' = loss modulus. [c] Tan $\delta = G''/G'$.

storage modulus (G') and the lower the value, the stronger the gel. As can be seen from Table 2, the gel from **2b** possessed the lowest tan δ value among all the gels. These also correlate well with the morphology of the gels, where it was observed that **2b** self-assembled through thinner entangled fibres compared to **2d** which formed thicker and less entangled fibres or **3′a** and **3′d** which self-assembled through sheet like structures.

Experimental investigations into the self-assembly mechanism

To understand the mechanism of self-assembly during gelation, the organogels from **2b**, **2d**, **3′a** and **3′d** were also characterized by FTIR analysis in their crystalline and gel forms (Fig. S9, ESI†). Comparison of the IR spectra of organogelators **2b**, **2d**, **3′a** and **3′d** in their solid crystalline forms with those of their corresponding gels showed a considerable shift to a higher wave number, indicating O–H bonds and confirming that H-bonding plays a very important role in the self assembly of gelators. The shift to the higher wave number in the gel state compared to that in the solid crystalline state can be explained by the fact that the packing in the crystalline state is much more compact due to stronger H-bonding than that in the gel state.

Additionally, wide angle X-ray diffraction (WXRD) experiments were carried out for the xerogels of **2b**, **2d**, **3′a** and **3′d** (Fig. S10, ESI†). The diffraction patterns of the *p*-xylene xerogels showed periodical peaks indicating lamellar organization. The xerogel of **2b** obtained in this case for *p*-xylene showed much more crystalline phases and less amorphous phases than the benzene xergel reported previously.[20] For the *p*-xylene xerogel of **2b**, sharp peaks at 2θ values of 20.1° and 21.5° corresponding to *d* spacing values of 4.4 Å and 4.1 Å, respectively, indicated H-bonding interactions.[23,24] Additionally, for the *p*-xylene xerogel of **2b**, a sharp reflection peak was obtained at a 2θ value of 23.6° corresponding to a *d* spacing value of 3.8 Å, suggesting π–π stracking during the self-assembly.[25] Similarly, the *p*-xylene xerogels of the compounds **2d**, **3′a** and **3′d** also showed peaks that could be interpreted as contributers of H-bonding interactions during the self assembly. Thus, for **2d**, sharp peaks at 2θ values of 19.1° and 21.3° corresponding to *d* spacing values of 4.6 Å and 4.2 Å, respectively, were observed; for the xerogel of **3′a**, peaks at 2θ values of 18.5°, 19.3°, and 20.3° corresponding to *d* spacing values of 4.7 Å, 4.6 Å and 4.3 Å, respectively, were observed and for the xerogel of **3′d**, peaks at 2θ values of 18.1° and 20.2° corresponding to *d* spacing values of 4.8 Å and 4.3 Å, respectively, were observed. Additional peaks for the *p*-xylene xerogels of **2d**, **3′a** and **3′d** at 2θ values of 23°, 23.5° and 24.2°, respectively, were also observed with the corressponding d values of 3.9 Å, 3.7 Å and 3.6 Å, indicating the involvement of π–π stacking during the self-assembly.

Theoretical studies of the self-assembly process

To clearly understand the mechanism of self-assembly during gelation and to gather information on the particular reason behind the aggregation pattern in the gel state, theoretical studies were performed on **2b**, **2d**, **3′a** and **3′d**. Density functional theory (DFT) calculations were performed using the Gaussian 09 program.[26] Optimisations were carried out with a hybrid exchange–correlation functional B3LYP.[27–29] The triple-ζ quality basis set (TZVP)[30] was used for oxygen, while the SVP basis set[31] was used for carbon and hydrogen. Corresponding figures were made using the Chemcraft[32] visualization program.

FTIR analysis and WXRD experiments suggested that the H-bonding interaction is the main reason behind self-assembly in **2b**, **2d**, **3′a** and **3′d**. However, π–π stacking is also possible. To pinpoint the reason behind the aggregation, we performed geometry optimisation of dimers with both H-bonding and π–π stacking interactions. All these optimisations are carried out without any symmetry constraint to obtain the minimum energy configuration which is confirmed by vibrational frequency computation. The absence of the imaginary mode of vibration has been ascertained. The optimisations of all four monomers were performed using all the possible initial guess structures. For **2b**, two possibilities have been examined. Both the initial guesses have converted to the most stable geometry (ΔE = 166 kcal mol^{-1}) (Fig. 3a). The optimised geometries of the other 3 monomers were also optimized similarly (Fig. S13–S15, ESI†).

The general assumptions for the gel formation of these types of aromatic compounds are association with π–π stacking interactions as well as H-bonding interactions. We have taken

Open Access Article. Published on 18 March 2022. Downloaded on 2/8/2026 1:46:29 AM.
This article is licensed under a Creative Commons Attribution-NonCommercial 3.0 Unported Licence.

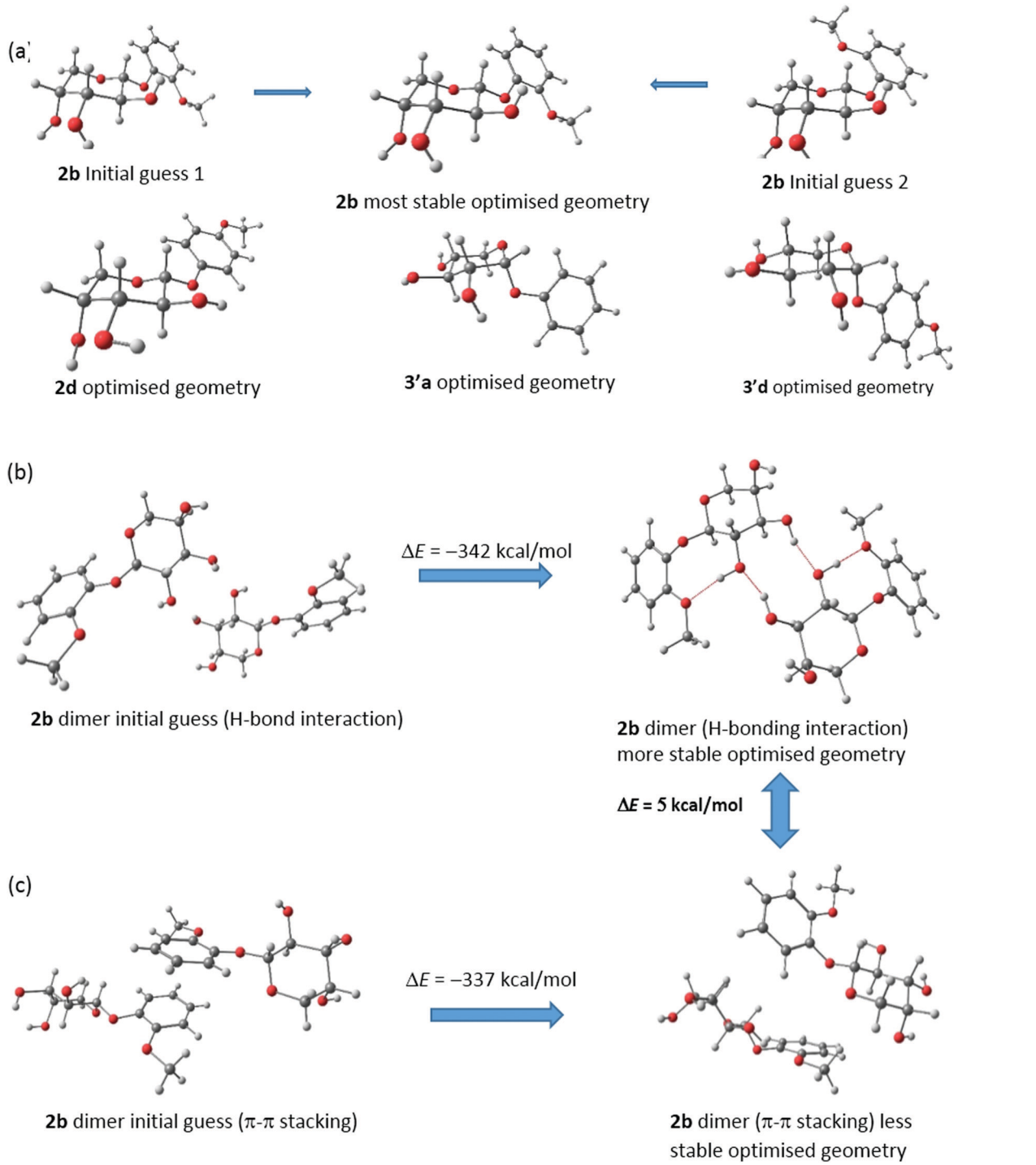

Fig. 3 (a) Optimized geometries of (a) monomers of **2b**, **2d**, **3′a** and **3′d**. Optimized geometries of two differently oriented dimers of **2b** by (b) H-bonding interactions (c) π−π stacking interactions.

both possibilities in mind and taken two differently oriented geometries of dimers. The first one deals with only π–π stacking whereas the second type includes the possibilities of H-bonding. Comparing the energy values of the optimised geometries, we found that the H-bonding interactions are more likely in the cases of **2b**, **2d**, **3′a** and **3′d**. Dimerization occurs predominantly through H-bonding interactions.

The optimisation of dimers of two different types shows that H-bonding interactions in **2b** are favourable over π–π stacking by 5 kcal mol^{-1}. In favour of this claim, we have presented the starting and optimised geometries of these two dimers and compared their energies (Fig. 3b and c). However, for both cases, final optimised geometries are heavily stabilised with respect to the initial guess structure and thus it is possible to

© 2022 The Author(s). Published by the Royal Society of Chemistry

Open Access Article. Published on 18 March 2022. Downloaded on 2/8/2026 1:46:29 AM.
This article is licensed under a Creative Commons Attribution-NonCommercial 3.0 Unported Licence.

have a smaller contribution of π–π stacking in the self-assembly process for gel formation which is also backed by our experimental findings with WXRD. Similar dimerization possibilities have also been studied for **2d**, **3′a** and **3′d** and are shown in Fig. S13–S15 (ESI†). Similar trends have been reported for these three cases. Distortions in the π–π stacking interactions throughout the optimisation process have been observed for all three compounds. Also, it is observed that, for **2b**, the H-bonding interactions are much stronger than for the other three compounds (**2d**, **3′a** and **3′d**) as additional H-bonds can be found. Further studies are being carried out considering the H-bonding interactions and forming three-dimensional structured aggregates with four monomers. The entrapment of curcumin is also being investigated using DFT studies with these initial findings.

Entrapment of curcumin in oragnogels and characterization of the curcumin-entrapped gel

Organogels have been explored as media for the controlled release of drugs for some time.[33–36] This application can be attributed to the fact that as smart materials organogels are responsive to various stimuli which can be used to trigger the release of the entrapped drugs. Such applications are mainly restricted to organogels of amino acids[37–40] and peptides,[41] phospholipids,[42] fatty acids[43] and their derivatives,[44] steroids[45] and alkylamides.[46] In contrast, carbohydrate based organogelators have rarely been explored for controlled release studies. Due to the importance of this area of research and the biocompatibility and eco-friendly nature of our organogels, we explored the controlled release of curcumin as a model drug, from the organogel of **2b**. Since the organic solvents that were gelled by **2b** are not biocompatible and toxic, we selected mustard oil as the medium for the curcumin release studies. The entrapment of curcumin into the **2b** gel was carried out by simply heating a solution of the former in mustard oil with the latter and then allowing the mixture to stand at ambient temperature till the gel formation was observed by the inversion test. From a series of experiments, it was determined that a maximum of 0.5% (w/v) of curcumin could be entrapped in the mustard oil gel and loading of curcumin beyond this resulted in the formation of a very unstable gel.

To gain insight into the effect of curcumin on the mechanical properties and stability of the mustard oil gels of **2b**, the native mustard oil gel and the mustard oil gel loaded with curcumin were subjected to rheological experiments (Fig. S11 and S12, ESI†). For this purpose, the results obtained from the DSS and DFS experiments of the mustard oil gel of **2b** at 1.5% (w/v) and the 1.5% curcumin loaded gels of **2b** with a gelator concentration of 1.5% (Table 3) were compared (Table 3). It was found that the value of γ for the curcumin loaded gel was slightly higher than that for the native gel. Also, the $\tan\delta$ value of the former was slightly lower than that of the latter, which indicated that the incorporation of curcumin into the gel led to a mechanically more robust gel. This could be due to the additional H-bonding interactions provided by the phenolic groups of curcumin and additional π–π interactions provided by the phenyl rings of curcumin during self-assembly, leading to more robust cross-linking. Again, the gelation of curcumin in the presence of sugars has also been reported to be induced which may also contribute to the enhanced mechanical properties observed in our case.[47]

Table 3 Rheological properties of the gels **2b** and **2b** + Cur in mustard oil

Gel	$G' \times 10^3$ (Pa)[a]	$G'' \times 10^3$ (Pa)[b]	$\gamma \times 10^{-2}$ (%)	Tan δ[c]
2b	11.96	1.74	4.42	0.14
2b + Cur	10.91	1.19	5.56	0.11

[a] G' = storage modulus. [b] G'' = loss modulus. [c] Tan $\delta = G''/G'$.

Curcumin release with pH as stimulus

Due to the precedence of the use of pH as a stimulus to control the release of drugs from gels,[48] we explored the controlled release of curcumin from the curcumin entrapped gel using the former as a trigger. The curcumin release experiments were carried out from the curcumin entrapped gel at different pH values using phosphate buffer solution (PBS) at 25 °C. The gelator–curcumin ratio was kept constant in all cases, wherein **2b** (20 mg) was mixed with curcumin (2.0 mg) and mustard oil (2 mL) in a 15 mL sample vial. Then the curcumin entrapped gel (**2b** + Cur) was prepared by warming the mixture to 50 °C to dissolve the solids after which it was left to stand at room temperature for the gel to form. Then 4 mL of phosphate buffer solution was added on top of the gel so that the curcumin could be released from the gel to the phosphate buffer (Fig. 4).

The release of curcumin from the gel medium to the phosphate buffer medium was monitored through UV-vis spectroscopy of the phosphate buffer at fixed intervals (Fig. 5a and Fig. S17–S20, ESI†). The graph for the comparative release of curcumin from the **2b** + Cur gel at different pH values is plotted in Fig. 5b. The data for the 100% release of curcumin are listed in Table 4. At a pH of 8, the curcumin release was very fast and within 5 hours 100% of the curcumin was released into the buffer medium. The release time of curcumin from the gel was found to increase with the decreasing pH of the buffer medium. Thus, for 100% release of the curcumin, the times taken were about 18 h at pH 7.6, about 27 h at pH 7.4, 33 h at pH 7 and about 49 h at pH 5.8. This led us to conclude that the gels were suitable for the slow release of curcumin through transdermal applications which are associated with a pH of 5–6. The release profiles of the curcumin from the gels were also seen to be strongly correlated with the gel degradation (Fig. 4). Again the degradation of the gel structure did not affect the chemical structure of the gelator at all the pH values studied, as the gelator could be re-isolated from the mixture after the study. Therefore, it can be concluded that the disruption of the self-assembly resulting in the degradation of the gel was related to the pH due to the decrease of the H-bonding necessary for the self-assembly, especially under the basic pH. From control studies, it was also observed that the gels were less stable in basic medium (96 h) than in acidic medium (>150 h). This was probably due to the disruption of the H-bonding responsible for self-assembly by strongly basic ions

Open Access Article. Published on 18 March 2022. Downloaded on 2/8/2026 1:46:29 AM.
This article is licensed under a Creative Commons Attribution-NonCommercial 3.0 Unported Licence.

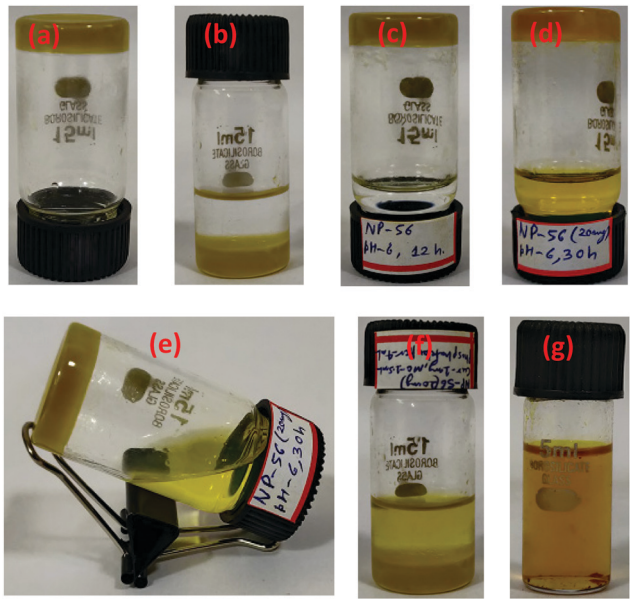

Fig. 4 Images of the curcumin release experiments: (a) gels of **2b** + Cur in MO; (b) gels of **2b** + Cur in MO and 4 mL phosphate buffer solution at pH 5.8; (c) after 12 h and (d) after 30 h; (e) biphasic mixture of **2b** + Cur in MO and phosphate buffer, after 30 h (f) and after 40 h release (g). The mixture after 49 h shows the complete degradation of the gel and no discernible separation of the oil and PBS layers.

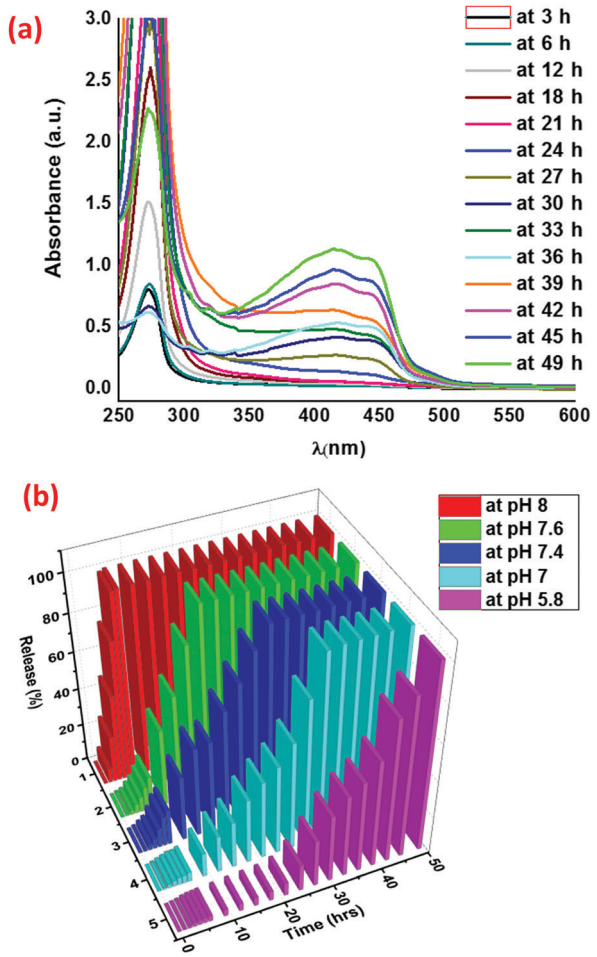

Fig. 5 (a) UV-Visible spectra of the release of curcumin from **2b** + Cur at pH 5.8 in phosphate buffer solution. (b) Comparative release profiles of curcumin at different pH values.

which themselves preferred to form H-bonds with the H-bond donor sites in the gelator. Again, curcumin is more soluble in a basic pH solution than in an acidic pH solution, and this could also contribute to its faster release in the basic pH solution compared to the acidic pH solution. Another factor that could contribute to the slower release in the acidic pH solution is the fact that the degree of protonation of curcumin or the gelator is much higher than in the basic pH solution. The increased protonation could also lead to a comparatively slower degradation of the gel at these pH values compared to the basic pH value.

Kinetics of the release of curcumin

The kinetic release profile plays a vital role in understanding the formulation concerning the release rates and to find out whether the drug release occurs in an understandable pattern. To gain an insight into the kinetics of the curcumin release from the gel at pH 5.8, the release data were analysed with hypothetical drug release kinetic approaches such as the zero-order kinetic plot and first-order kinetics plot (Fig. S21a and S22, ESI†).[49] The approximation accuracy of individual models was evaluated in terms of the correlation coefficient (R^2) value. In the case of zero-order kinetics (Fig. S21, ESI†), the data obtained were plotted as the cumulative drug release *vs.* time; the R^2 value of the release was found to be 0.8594 which is less than the R^2 value of 0.9486 obtained from the plot of the first-order kinetics (Fig. S22, ESI†). This could possibly be indicative of the release of the curcumin from the gel by first order kinetics with respect to the former. However, from a closer inspection of the data for the release *via* zero-order kinetics, it can be observed that the initial release up to nearly 20 h was associated with a very low release, which increased sharply subsequently. Therefore, assuming that the release occurred in two stages, a linear fit of the zero-order kinetics data from 20 h onwards was made (Fig. S21b, ESI†). This was associated with a correlation factor of 0.9879, which is higher than that of the linear fit from the first-order kinetics. Therefore, the release can also be explained by the zero-order kinetics model if we ignore the initial 20 h of the release during which time the actual release was very low.[50] Such a release may be associated with the stability of the gel with respect to time. Initially, the gel was stable and the release was very slow. Subsequently, with the degradation of the gel, the release accelerated. The disintegration

Table 4 Time for 100% curcumin release at different pH values

	2b + Cur ratio (4 : 1, 10 mg for each experiment), volume of mustard oil (1 mL)				
	pH 5.8	pH 7.0	pH 7.4	pH 7.6	pH 8.0
Curcumin release time	49 h	33 h	27 h	18 h	5 h

© 2022 The Author(s). Published by the Royal Society of Chemistry

Open Access Article. Published on 18 March 2022. Downloaded on 2/8/2026 1:46:29 AM.
This article is licensed under a Creative Commons Attribution-NonCommercial 3.0 Unported Licence.

of the gel starts to operate at a similar time interval and then is rapidly accelerated resulting in an increase of the regression coefficient. Notably, during the drug release experiment, the degradation and erosion of the gel phase could be visually detected (Fig. 4). The degradation of the gel structure was also detected through the absorption studies where the presence of gelator in the release medium could be detected through UV-vis spectra, thus confirming that the erosion of the gel was a major contributor towards the release of curcumin. Therefore, a complex mechanism of the curcumin release involving the degradation of the gel in multiple steps involving diffusion, the erosion of the gel and the formation of oil in PBS emulsions/micelles seems to be operative. Initially, the release may be through a diffusion mechanism and as with time the gel degraded, the release became faster with the concomitant formation of oil encapsulated emulsions/micelles, as is evident from Fig. 4g where no discernible boundary was visible between the oil and PBS layers.

Conclusions

In this work, we have explored the gelation ability of a library of phenolic glycosides of pentose sugars, wherein it was found that β-arabinoses (**2b** and **2d**) and α-xylosides (**3′a** and **3′d**) were able to act as organogelators. Again with respect to the substituents on the phenols in the arabino-series, it was seen that the *ortho*-methoxy substituted phenolic arabinoside **2b** formed a mechanically more robust gel than the *para*-methoxy substituted phenolic arabinoside **2d**. Similarly, in the xylo series, the unsubstituted phenolic xyloside **3′a** formed a mechanically more robust gel than the *para*-methoxy substituted phenolic xyloside **3′d**. All the gels were characterized through a variety of techniques and it was observed that the mechanical strength of the gels correlated with the morphology of the gel structure. The self-assembly of the gelators occurred mostly through H-bonding forces although some evidence of π–π stacking was also observed. This was evident from experimental studies such as FTIR spectroscopy and WXRD and was reinforced through theoretical modelling studies. The mechanical strength of the organogels from the *ortho*-methoxyphenol β-glycoside of arabinose **2b** was found to be greater than those for the *para*-derivative **2d** or the corresponding xyloside gels from **3′a** and **3′d**. This observation correlates well with our previous studies where we have reported several structurally simple β-arabinoside derivatives as LMOGs at very low concentrations. Organogelator **2b** was also able to gel mustard oil, a feature that was used to entrap curcumin in a gel matrix for potential application as a controlled release medium. Entrapment of curcumin in the **2b**-mustard organogel led to an increase in the robustness of the gel, possibly through the contribution of the phenolic hydroxyls of curcumin leading to greater cross-linking of the self-assembled **2b** fibres. The release of curcumin was explored in media with different pH values and it was found that the slowest release occurred at pH 5.8, implying that **2b**-curcumin could be potentially used for transdermal applications. The curcumin release was associated with the degradation of the gel medium and followed first order kinetics with respect to time.

Author contributions

Navendu P. Pathak carried out the experimental work and wrote the preliminary draft of the manuscript. Arunava Sengupta was responsible for the theoretical modelling studies. Somnath Yadav was responsible for the conceptualization of the work, generating funds, the overall supervision of the project and writing the final version of the manuscript.

Conflicts of interest

There are no conflicts to declare.

Acknowledgements

The authors thank the Council for Scientific and Industrial research (CSIR), India [grant number 02(0362)/19/EMR-II], for financial support.

Notes and references

1 N. Zweep and J. H. van Esch, The design of molecular gelators. In *Functional molecular gels*, ed. B. Escuder and J. F. Miravet, Royal Society of Chemistry: UK, 2013; Vol 1, pp 1–3.
2 P. Dastidar, *Gels*, 2019, **5**, 15.
3 O. Gronwald and S. Shinkai, *Chem. – Eur. J.*, 2001, **7**, 4328–4334.
4 S. Datta and S. Bhattacharya, *Chem. Soc. Rev.*, 2015, **44**, 5596–5637.
5 J. Morris, J. Bietsch, K. Bashaw and G. Wang, *Gels*, 2021, **7**, 24.
6 N. Basu, A. Chakraborty and R. Ghosh, *Gels*, 2018, **4**, 52.
7 O. Gronwald, K. Sakurai, R. Luboradzki, T. Kimura and S. Shinkai, *Carbohydr. Res.*, 2001, **331**, 307–318.
8 K. Yoza, N. Amanokura, Y. Ono, T. Akao, H. Shinmori, M. Takeuchi, S. Shinkai and D. Reinhoudt, *Chem. – Eur. J.*, 1999, **5**, 2722–2729.
9 K. Yoza, Y. Ono, K. Yoshihara, T. Akao, H. Shinmori, M. Takeuchi, S. Shinkai and D. N. Reinhoudt, *Chem. Commun.*, 1998, 907–908.
10 R. Luboradzki, O. Gronwald, M. Ikeda, S. Shinkai and D. N. Reinhoudt, *Tetrahedron*, 2000, **56**, 9595–9599.
11 D. Wang, A. Chen, J. Morris and G. Wang, *RSC Adv.*, 2020, **10**, 40068–40083.
12 J. Morris, P. Kozlowski and G. Wang, *Langmuir*, 2019, **35**, 14639–14650.
13 A. Chen, D. Wang, L. P. Samankumara and G. Wang, *Synthesis*, 2019, 2897–2908.
14 A. Chen, L. P. Samankumara, C. Garcia, K. Bashaw and G. Wang, *New J. Chem.*, 2019, **43**, 7950–7961.
15 A. Chen, I. S. Okafor, C. Garcia and G. Wang, *Carbohydr. Res.*, 2018, **461**, 60–75.

Open Access Article. Published on 18 March 2022. Downloaded on 2/8/2026 1:46:29 AM.
This article is licensed under a Creative Commons Attribution-NonCommercial 3.0 Unported Licence.

16 A. Chen, S. B. Adhikari, K. Mays and G. Wang, *Langmuir*, 2017, **33**, 8076–8089.
17 G. Wang, N. Goyal, H. P. R. Mangunuru, H. Yang, S. Cheuk and P. V. N. Reddy, *J. Org. Chem.*, 2015, **80**, 733–743.
18 N. Goyal, H. P. R. Mangunuru, B. Parikh, S. Shrestha and G. Wang, *Beilstein J. Org. Chem.*, 2014, **10**, 3111–3121.
19 A. Chen, D. Wang, J. Bietsch and G. Wang, *Org. Biomol. Chem.*, 2019, **17**, 6043–6056.
20 N. P. Pathak, Rajkamal and S. Yadav, *Chem. Commun.*, 2020, **56**, 2999–3002.
21 Rajkamal, D. Chatterjee, A. Paul, S. Banerjee and S. Yadav, *Chem. Commun.*, 2014, **50**, 12131–12134.
22 Rajkamal, N. P. Pathak, T. Halder, S. Dhara and S. Yadav, *Chem. – Eur. J.*, 2017, **23**, 11323–11329.
23 Rajkamal, N. P. Pathak, D. Chatterjee, A. Paul and S. Yadav, *RSC Adv.*, 2016, **6**, 92225–92234.
24 S. S. Babu, V. K. Praveen and A. Ajayghosh, *Chem. Rev.*, 2014, **114**, 1973–2129.
25 D. K. Maiti and A. Banerjee, *Chem. – Asian J.*, 2013, **8**, 113–120.
26 M. J. Frisch, G. W. Trucks, H. B. Schlegel, G. E. Scuseria, M. A. Robb, J. R. Cheeseman, G. Scalmani, V. B. Izmaylov, B. Mennucci, G. A. Petersson, H. Nakatsuji, M. Caricato, X. Li, H. P. Hratchian, A. F. Izmaylov, J. Bloino, G. Zheng, J. L. Sonnenberg, M. Hada, M. Ehara, K. Toyota, R. Fukuda, J. Hasegawa, M. Ishida, T. Nakajima, Y. Honda, O. Kitao, H. Nakai, T. Vreven, Jr. J. A. Montgomery, J. E. Peralta, F. Ogliaro, M. Bearpark, J. J. Heyd, E. Brothers, K. N. Kudin, V. N. Staroverov, R. Kobayashi, J. Normand, K. Raghavachari, A. Rendell, J. C. Burant, S. S. Iyengar, J. Tomasi, M. Cossi, N. Rega, N. J. Millam, M. Klene, J. E. Knox, J. B. Cross, V. Bakken, C. Adamo, J. Jaramillo, R. Gomperts, R. E. Stratmann, O. Yazyev, A. J. Austin, R. Cammi, C. Pomelli, J. W. Ochterski, R. L. Martin, K. Morokuma, V. G. Zakrzewski, G. A. Voth, P. Salvador, J. J. Dannenberg, S. Dapprich, A. D. Daniels, Ö. Farkas, J. B. Foresman, J. V. Ortiz, J. Cioslowski and D. J. Fox, *Gaussian 09, revision C.01*, Gaussian, Inc., Wallingford, CT, 2010.
27 A. D. Becke, *J. Chem. Phys.*, 1993, **98**, 5648–5652.
28 C. Lee, W. Yang and R. G. Parr, *Phys. Rev. B: Condens. Matter Mater. Phys.*, 1998, **37**, 785–789.
29 P. J. Stevens, F. J. Devlin, C. F. Chabalowski and M. J. Frisch, *Phys. Chem.*, 1994, **98**, 11623–11627.
30 A. Schafer, C. Huber and R. Ahlrichs, *J. Chem. Phys.*, 1994, **100**, 5829–5835.
31 A. Schafer, H. Horn and R. Ahlrichs, *J. Chem. Phys.*, 1992, **97**, 2571–2577.
32 http://www.chemcraftprog.com/.
33 J. Bietsch, M. Olson and G. Wang, *Gels*, 2021, **7**, 134.
34 C. L. Esposito, P. Kirilov and V. G. Roullin, *J. Controlled Release*, 2018, **271**, 1–20.
35 J. Mayr, C. Saldias and D. D. Diaz, *Chem. Soc. Rev.*, 2018, **47**, 1484–1515.
36 S. S. Sagiri, B. Behera, R. R. Rafanan, C. Bhattacharya, K. Pal, I. Banerjee and D. Rousseau, *Soft Mater.*, 2014, **12**, 47–72.
37 M. Khuphe, B. Mukonoweshuro, A. Kazlauciunas and P. D. Thornton, *Soft Matter*, 2015, **11**, 9160–9167.
38 S. Kaplan, M. Colak, H. Hosgoren and N. Pirinccioglu, *ACS Omega*, 2019, **4**, 12342–12356.
39 B. Hu, W. Sun, H. Li, H. Sui and S. Li, *Int. J. Pharm.*, 2018, **547**, 637–647.
40 B. Hu, H. Yan, Y. Sun, X. Chen, Y. Sun, S. Li, Y. Jing and H. Li, *Artif. Cells, Nanomed., Biotechnol.*, 2020, **48**, 266–275.
41 W. Gao, Y. Liang, X. Peng, Y. Hu, L. Zhang, H. Wu and B. He, *Biomaterials*, 2016, **105**, 1–11.
42 G. Bayer, S. Grasselli, A. Malchiodi and I. S. Bayer, *Colloids Surf., A*, 2021, **619**, 126537.
43 E. Yadav, A. K. Khatana, S. Sebastian and M. K. Gupta, *New J. Chem.*, 2021, **45**, 415–422.
44 B. Martin, F. Brouillet, S. Franceschi and E. Perez, *AAPS PharmSciTech*, 2017, **18**, 1261–1269.
45 A. K. Bandela, V. K. Hinge, D. S. Yarramala and C. P. Rao, *ACS Appl. Mater. Interfaces*, 2015, **7**, 11555–11566.
46 S. Uzan, D. Barıs, M. Colak, H. Aydın and H. Hosgoren, *Tetrahedron*, 2016, **72**, 7517–7525.
47 S. Wong, J. Zhao, C. Cao, C. K. Wong, R. P. Kuchel, S. De Luca, J. M. Hook, C. J. Garvey, S. Smith, J. Ho and M. H. Stenzel, *Nat. Commun.*, 2019, **10**, 582.
48 R. Pan, G. Liu, Y. Zeng, X. He, Z. Ma, Y. Wei, S. Chen, L. Yang and L. Tao, *Polym. Chem.*, 2021, **12**, 2457–2463.
49 R. Gouda, H. Baishya and Z. Qing, *J. Dev. Drugs*, 2017, **6**, 2–10.
50 P. J. Haddow, M. A. da Silva, D. B. Kaldybekov, C. A. Driess, E. Hoffman, V. Hutter, V. V. Khutoryanskiy, S. B. Kirton, N. Mahmoudi, W. J. McAuley and M. T. Cook, *Macromol. Biosci.*, 2021, 2100432.

© 2022 The Author(s). Published by the Royal Society of Chemistry